J. Fluid Mech. (1990), *vol.* 216, *pp.* 411–435
Printed in Great Britain

Linear-eddy modelling of turbulent transport. Part 3. Mixing and differential molecular diffusion in round jets

By ALAN R. KERSTEIN
Combustion Research Facility, Sandia National Laboratories, Livermore, CA 94551-0969, USA

(Received 10 July 1989)

The linear-eddy model of turbulent mixing represents a spatially developing flow by simulating the time development along a comoving transverse line. Along this line, scalar quantities evolve by molecular diffusion and by randomly occurring spatial rearrangements, representing turbulent convection. The modelling approach, previously applied to homogeneous turbulence and to planar shear layers, is generalized to axisymmetric flows. This formulation captures many features of jet mixing, including differential molecular diffusion effects. A novel experiment involving two unmixed species in the nozzle fluid is proposed and analysed.

1. Introduction

Multidimensional models of chemically reacting turbulent shear flows, involving large-eddy simulation, p.d.f. closure, or other methods, cannot affordably resolve all relevant lengthscales of the mixing field at Reynolds numbers of practical interest. A multidimensional model therefore requires a mixing submodel such as Curl's (1963) coalescence-dispersion model to represent the combined influence of molecular diffusion and convective stirring at the unresolved lengthscales. Because the mechanistic distinction between these two influences is absent, the representation of Schmidt-number (*Sc*) effects is problematic (Pope 1985). The consequent practical difficulties are evident in efforts to model the measured differences between gaseous and liquid mixing in turbulent flows (Givi, Ramos & Sirignano 1985).

Such differences have been highlighted by an extensive experimental study of gaseous and liquid planar mixing layers, summarized by Broadwell & Dimotakis (1986). For turbulent round jets, measurements suitable for at least a preliminary comparison of gaseous and liquid mixing have been performed (Dahm 1985; Papantoniou 1985; Dowling 1988). (Highlights of these investigations are reported by Dahm & Dimotakis 1987, Papantoniou & List 1989, and Dowling & Dimotakis 1990.) Another indication of *Sc* sensitivity in turbulent jets is provided by recent measurements of differential molecular diffusion in a jet of H_2 and Freon into air (Kerstein *et al.* 1989).

The linear-eddy modelling approach, designed to overcome the aforementioned deficiency of mixing submodels, was originally formulated in the context of a model of mixing in homogeneous turbulence (Kerstein 1988). A generalization to planar shear layers was found to reproduce measured *Sc* effects as well as Reynolds-number *Re* and Damköhler-number *Da* effects (Kerstein 1989). For application to round jets, the approach is generalized here to axisymmetric geometries, and jet similarity scalings are incorporated.

The paper is organized as follows. The linear-eddy modelling concept is briefly reviewed, and an axisymmetric formulation is introduced. This formulation is used to compute spatially resolved fluctuation statistics for turbulent scalar mixing in gaseous ($Sc = 0.7$) and liquid ($Sc = 600$) jets for Re_{jet} ranging over a factor of 10^3. Next, predictions of differential molecular diffusion effects are presented for a jet of H_2 and propane ($Sc = 0.18$ and 1.2, respectively) into air. Finally, a novel experiment involving two unmixed species in the nozzle fluid is proposed and analysed. These results are compared to measurements and to the predictions of other models.

2. Model formulation and implementation

2.1. *The linear-eddy modelling approach*

To preserve the mechanistic distinction between small-scale convective stirring and molecular diffusion, thereby capturing Sc effects, the approach that is adopted is to resolve all relevant lengthscales in a stochastic simulation of turbulent mixing. For Re of practical interest, of order 10^4 for free shear flows, this is affordable only in a one-dimensional computation. The computational domain is chosen to be a line transverse to the mean flow. (For some applications it is preferable to choose a streamwise line (Kerstein 1986).) The simulated time evolution of the scalar field on this line represents the spatial development of the scalar field along a transverse line moving with the mean flow. Thus, each simulated realization is analogous to a planar snapshot of the flow, with the streamwise coordinate parameterized by the simulation time. For the planar shear-layer application, the transverse line is the coordinate normal to the splitter plate (Kerstein 1989). For the round jet, the transverse line is the radial coordinate. Except for modifications needed to accommodate the axisymmetric geometry and jet similarity scalings, the model formulation is the same as for the shear-layer application. That formulation is summarized briefly. Details omitted from the present discussion are provided in the aforementioned reference.

A simulated realization of the scalar field on the transverse line evolves from its initial state by means of two concurrent mechanisms. One mechanism, molecular diffusion, is implemented deterministically based on Fick's law. If multiple species are incorporated, as in simulations of differential-diffusion effects, the molecular diffusivity D_{M} is assigned a different value for each species. The resolution of all relevant lengthscales allows this mechanism to be implemented without approximation. (For multicomponent diffusion, the appropriate generalization of Fick's law can be incorporated, but this is not implemented here.)

The other mechanism, convective stirring, is simulated on the transverse line by means of a stochastic rearrangement process, rather than by solving a fluid-mechanical equation. The rearrangement process is formulated so as to incorporate the distribution of length- and timescales specified by the Kolmogorov cascade picture of inertial-range turbulence. The rearrangement process consists of a sequence of randomly occurring 'block-inversion' events. Each event consists of the random selection of a block (a size-l interval) along the line, and instantaneous inversion of the scalar field within the block. Namely, the scalar field $\xi(r)$ is replaced by $\xi(2r_0 - r)$ for $|r - r_0| < \frac{1}{2}l$, but is unchanged for $|r - r_0| > \frac{1}{2}l$, where r_0 is the block centre. (This formulation, suitable for planar symmetry, is modified in §2.2 for application to axisymmetric flows.) This mirror-image mapping with respect to the block centre represents the effect of an individual size-l eddy on the scalar field. (For an illustrative example, see figure 1 of Kerstein 1988.)

Reflecting the analogy between blocks and inertial-range eddies, the block size is a random variable confined to the range $L_K < l < L$, where L is the integral scale and L_K is the Kolmogorov scale. The block-size probability density function (p.d.f.) $f(l)$ is assigned by requiring that the turbulent diffusivity induced by blocks smaller than a given size l_0 should be proportional to $l_0^{\frac{4}{3}}$, consistent with the Kolmogorov cascade picture. The model analogue of turbulent diffusivity is the diffusivity associated with the random walk of a passive marker particle under the influence of a succession of block-inversion events. Based on a straightforward random-walk analysis (Kerstein 1989), the contribution to marker diffusivity due to blocks in the size range $(l, l+\mathrm{d}l)$ is $\frac{1}{6}\lambda l^3 f(l)\,\mathrm{d}l$, where λ is the rate of occurrence of block-inversion events per unit interval along the transverse line. The generalization to a spatially varying event rate $\lambda(r)$ for inhomogeneous flow is discussed in §2.2.

Adoption of the Kolmogorov scaling yields

$$f(l) = \frac{5}{3L}\frac{1}{(L/L_K)^{\frac{5}{3}}-1}\left(\frac{l}{L}\right)^{-\frac{5}{3}}, \tag{1}$$

where the l-dependence follows from the scaling and the prefactor is obtained from normalization over the range $L_K < l < L$.

To express λ in terms of physical quantities, an expression for the turbulent diffusivity is required. Omitting empirical coefficients of order unity, the turbulent diffusivity is taken to be

$$D_T = \nu Re = \nu(L/L_K)^{\frac{4}{3}}, \tag{2}$$

where ν is the kinematic viscosity and Re is the turbulence Reynolds number, specified for the round jet in §2.2. The second equality reflects inertial-range scaling. The foregoing results give (Kerstein 1989)

$$\lambda = \frac{24}{5}\frac{\nu}{L^3}\left(\frac{L}{L_K}\right)^3 \tag{3}$$

to leading order in $L/L_K \gg 1$.

It is evident that the model is a turbulent mixing analogy rather than a hydrodynamic model *per se*, since stirring occurs by means of a rearrangement process with no explicitly defined velocity field. Parameters governing the rearrangement process must therefore be assigned based on empirically determined properties of the flow field, in particular the spatial variation of Re and L, as elaborated in §2.2. The model thus simulates the evolution of the scalar field under the influence of the specified mixing process. Although an empirical specification of the gross structure of the flow field is required, empirical coefficients are omitted, for example, from (2) because the intent of the model is to reproduce and interpret measured features and trends, rather than precise numerical values. The objective is to ascertain whether those features and trends reflect a generic mixing process or whether details of the mixing process are configuration-specific.

In this spirit, flow-field properties are assigned in accordance with the similarity scalings governing the flow configuration. Near-field effects associated with, for example, the potential core of the jet are thus omitted. The model exhibits near-field transients reflecting the relaxation of the scalar field to similarity form under the influence of the rearrangement process, but these transients do not necessarily correspond to measured near-field transients. In particular, the simulated scalar field relaxes to similarity more rapidly than in the actual flow.

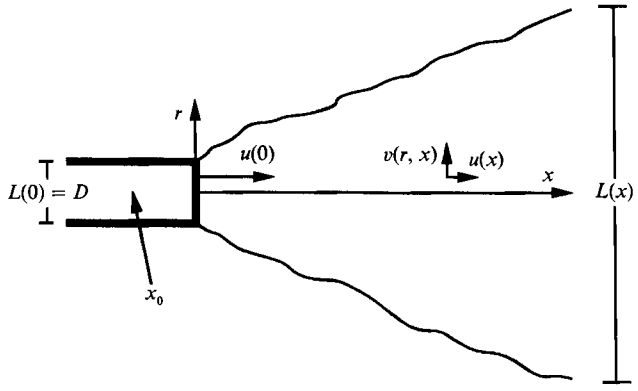

FIGURE 1. Schematic illustration of the round jet.

2.2. *Adaption to the turbulent round jet*

The picture of turbulent round jet development that is adopted here is illustrated in figure 1. Fluid issues from a nozzle of diameter D into a quiescent medium (i.e. no coflow) of the same density and viscosity. (Note that a subscripted D denotes a diffusivity.) Adopting round-jet similarity scalings (Landau & Lifshitz 1959), the centreline mean velocity decreases with downstream distance according to

$$\frac{u(0)}{u(x)} = c\left(\frac{x-x_0}{D}\right), \tag{4}$$

where $u(0)$ is the nozzle velocity. The scaling factor c and the effective origin x_0 are sensitive to nozzle design, and their measured values vary considerably (Gouldin *et al.* 1986). Here, the representative value $c = 0.2$ is adopted, and x_0/D is set equal to $-1/c = -5$ so that mean-flow similarity is satisfied for all $x > 0$.

Within the turbulent zone, radial variation of the axial component $u(x, r)$ of the mean velocity is neglected, and $u(x, r)$ is assigned the centreline value $u(x)$ specified by (4). This and related simplifying assumptions, specified shortly, are adopted with the intent of ascertaining whether key features of the mixing process in turbulent jets can be reproduced without explicitly incorporating the multidimensional nature of the flow field.

The computational domain represents a radial line corresponding to the range $-L(x) < r < L(x)$, where $L(x)$ is a characteristic scale of the turbulent zone. Concretely, the simulated scalar field at any instant is analogous to an instantaneous measurement of the scalar field along a radial line. The axial location x of the radial line is parameterized by the computational time t according to

$$\frac{\mathrm{d}x}{\mathrm{d}t} = u(x). \tag{5}$$

Based on the mapping defined by (4) and (5), x and t are henceforth used interchangeably.

Similarity requires linear growth of the characteristic scale $L(x)$ of the turbulent zone, namely

$$L(x) = c(x-x_0). \tag{6}$$

Here, $L(x)$ is interpreted both as the integral scale of the turbulence (i.e. the size of

the largest eddies) and as the local width of the vortical zone. The former interpretation leads to the identification of $L(x)$ as upper bound L on the range of block sizes, as defined in (1). The latter interpretation motivates the specification of the block-inversion event rate $\lambda(r)$, defined above (1). Blocks may be viewed as eddies with vorticity concentrated at the block centres. Therefore the block centres are confined to the vortical zone, namely the radial interval $-\frac{1}{2}L < r < \frac{1}{2}L$. Within this zone, radial variation of the turbulent diffusivity is neglected, so $\lambda(r)$ has the value given by (3) within the vortical zone, and is zero outside that zone.

As a consequence of this formulation, the zone to which blocks are confined is twice as large as the zone to which their centres are confined. For the shear-layer application, this formulation was motivated by the experimental observation (Brown & Roshko 1974) that the vorticity thickness of a planar shear layer is roughly half the visual thickness. Consistent with the present objective of achieving a generic description of turbulent mixing in free-shear flows, this aspect of the shear-layer formulation is adopted here. The prevalence of large eddies capable of entraining parcels of fluid well beyond the vortical zone is a feature common to free-shear flows, although their 'coherent structure' and related properties are configuration-dependent.

It is instructive to express (3) in terms of Re (based on (2)), L, and the large-eddy turnover time $\tau = L/v'$, where v' is the r.m.s. fluctuation of the radial velocity component. It is appropriate to express turbulence quantities in terms of that component since the model incorporates only the radial fluctuations. Taking $D_T = v'L$ in (2), (3) becomes

$$\lambda = \frac{24}{5L\tau} Re^{\frac{5}{4}}. \tag{7}$$

This expression indicates that it is convenient to scale length and time by L and τ, respectively. Both of these quantities vary with x. In particular, τ, which may be expressed as $L^2/D_T = L^2/(\nu Re)$, is proportional to L^2 since jet similarity requires Re to be constant.

For the self-similar jet, the jet Reynolds number $Re_{\text{jet}} = u(x)L(x)/\nu$ is likewise constant. For purposes of comparison to measurements involving jets which typically are not self-similar at small x/D, the jet Reynolds number is taken to be $Re_{\text{jet}} = u(0)D/\nu$. The measurements of Wygnanski & Fiedler (1969) indicate that the ratio v'/u is roughly 0.25 along the jet centreline in the similarity region. Therefore the turbulence Reynolds number is taken to be $Re = \frac{1}{4}Re_{\text{jet}}$.

The x-dependence of the axial component u of the mean velocity implies a mean radial flow, by continuity. Expressed in cylindrical coordinates, continuity requires that the radial mean velocity component v satisfy

$$\frac{v}{r} + \frac{\partial v}{\partial r} = -\frac{\partial u}{\partial x}. \tag{8}$$

Taking u to be independent of r, as assumed earlier, (8) gives

$$v = -\frac{r}{2}\frac{\partial u}{\partial x}. \tag{9}$$

This mean radial flow is incorporated into the model by stretching the scalar field at a rate prescribed by (9). Stretching is implemented deterministically by means of dilatation events at regular time intervals. Each event involves the reassignment of

the scalar value of each computational cell to the cell or cells specified by the dilatation factor for that event. (Since $v(r,x)$ is proportional to r for given x, the computational domain is stretched by the same multiplicative factor for all r.) Owing to discretization of the computational domain, the scalar value in a given cell may be reassigned to more than one cell. (An alternative approach involving interpolation is not adopted because it would introduce numerical diffusion, causing a spurious enhancement of molecular diffusion.) By thus incorporating radial flow, the algorithm conserves total scalar flux, corresponding to the quantity

$$\pi u(x)\int_{-\infty}^{\infty}|r|\,\xi(r,x)\,\mathrm{d}r$$

in the simulation. For this quantity to be independent of x, the integral over the scalar field must increase as $1/u(x)$. The stretching process has precisely this effect.

Since the largest allowed block size is $L(x)$ and the largest allowed radial displacement of a block centre is $\frac{1}{2}L(x)$, the transverse range subject to block inversions is $-L(x) < r < L(x)$. Therefore the computational domain is limited to this range. Taking the scalar $\xi(r,t)$ to represent the nozzle-fluid mixture fraction, the initial condition for a simulated realization is $\xi(r,0) = 1$ for $|r| < \frac{1}{2}D$, $\xi(r,0) = 0$ for $|r| > \frac{1}{2}D$. As $L(x)$ increases, the computational domain widens, with a scalar value $\xi = 0$ assigned to newly incorporated cells, representing newly entrained fluid. Although in principle the molecular diffusion and stretching processes can transport nozzle fluid to r values beyond the specified computational domain, computed results do not change significantly when a larger domain is chosen, indicating that the specified domain is adequate.

Thus far, axisymmetry has been explicitly incorporated into the model only in the formulation of the continuity condition, (8), that determines the radial flow. The molecular diffusion process is implemented in accordance with axisymmetry by likewise formulating Fick's law for $\xi(r,t)$ in cylindrical coordinates, namely

$$\frac{\partial\xi}{\partial t} = \frac{D_{\mathrm{M}}}{r}\frac{\partial}{\partial r}\left(r\frac{\partial\xi}{\partial r}\right). \tag{10}$$

Equations (8) and (10) both reflect the fact that the volume of the annular region $r_1 < r < r_1+\mathrm{d}r$, $x_1 < x < x_1+\mathrm{d}x$ is $2\pi|r_1|\,\mathrm{d}r/\mathrm{d}x$, implying that a given scalar concentration $\xi(r_1)$ in a cell of width $\mathrm{d}r$ corresponds to a larger volume element of the scalar at larger $|r_1|$.

This consideration must also be reflected in the block-inversion process in order to conserve the scalar. The definition of a block-inversion event in §2.1 is modified as follows to incorporate axisymmetry. Denoting the block centre and block size as r_0 and l, respectively, the scalar value at r_0-y (where $0 < y < \frac{1}{2}l$) is assigned to location r_0+y only if $|r_0-y|/|r_0+y| > p$, where the value $0 < p < 1$ for a given event is randomly selected (i.e. p is uniformly distributed over $(0,1)$). In the ensemble average, this procedure corresponds to exchange of equal volume elements, thus conserving the scalar in the mean. For instance, if $|r_0-y| < |r_0+y|$, then the mean volume-element transfer per unit azimuthal angle from location r_0-y to location r_0+y is $|r_0+y|\,\mathrm{Prob}\,[|r_0-y|/|r_0+y| > p]\,\mathrm{d}r\,\mathrm{d}x$. Based on the definition of p, this equals $|r_0-y|\,\mathrm{d}r\,\mathrm{d}x$, which is equal to the volume-element transfer per unit azimuthal angle from r_0+y to r_0-y.

Satisfying scalar conservation in the mean rather than in each inversion event is a reasonable representation of scalar field measurements along a radial line. This is

because the measured scalar is conserved instantaneously when integrated over the entire flow field, but not when integrated over a control volume that exchanges material with other parts of the flow field.

Alternative, deterministic rules that conserve the scalar instantaneously along the radial line can be formulated, but they introduce undesirable artifacts. For instance, block inversion can be accompanied by a nonlinear transformation (i.e. longitudinal stretching and compression) of the scalar field within the block, specified by requiring that $r_1\,\mathrm{d}r_1 = r_2\,\mathrm{d}r_2$ for an exchange of scalar values at respective locations r_1 and r_2. This approach causes systematic changes in the radial derivative of the scalar, depending in a complicated way on r_0 and l. Such an artifact is particularly undesirable in a mixing model in which molecular-diffusive fluxes are driven by concentration gradients. This and related approaches are therefore deemed inappropriate.

2.3. *Implementation*

The concurrent processes of dilatation, molecular diffusion, and block inversion (viewed as a random point process in the time domain) are defined on a one-dimensional continuum. For computational purposes, the radial coordinate is discretized into cells small enough so that the spatial discretization does not have a significant impact on the computed results. Adequacy of the spatial resolution is verified by recomputing selected cases at higher resolution. In the computations reported here, the cell size Δr ranges from $0.00125D$ for liquid at high Re to $0.005D$ for gas at low Re. Molecular diffusion is implemented as a finite-difference solution of (10) with computational time step $\Delta t = 0.2(\Delta r)^2/D_{\mathrm{M}}$. For multispecies applications, Δt is assigned based on the largest of the species diffusivities.

Spatially resolved statistics of the fluctuating scalar field are gathered by running a number of realizations for each condition, parameterized by Re and Sc (with more than one Sc value for multispecies cases). Run-to-run variation of $\xi(r,t)$ reflects the random assignment of the times, locations, and p-values (defined in §2.2) of the block-inversion events. The reported results are based on a minimum of 200 realizations for each condition.

It should be noted that the only empirical inputs to the model are the similarity scaling factor $c = 0.2$ and the relationship $Re = \frac{1}{4}Re_{\mathrm{jet}}$.

3. Scalar mixing

3.1. *Mean and instantaneous profiles*

The cases that were computed are indicated in table 1. The range of x/D for which computed results are presented is shown for each case. Except for the differential-diffusion cases discussed in §4, all plotted results for a given case are denoted by the same symbol, irrespective of the x/D-value. For a given case, collapse of the data with respect to the radial similarity coordinate $\eta = r/(x-x_0)$ indicates similarity with respect to x/D. Similarity with respect to Re or Sc is indicated by comparisons among cases.

The cases $Re_{\mathrm{jet}} = 5000$ and $Re_{\mathrm{jet}} = 20000$ are of greatest practical interest because they span the range of the experimental work most relevant for data comparisons. The cases $Re_{\mathrm{jet}} = 100000$ for air and $Re_{\mathrm{jet}} = 100$ for water are included because their Péclet numbers (Pe) are almost equal, so they allow a Sc comparison with Pe effects essentially eliminated. The case of $Re_{\mathrm{jet}} = 100$ for air corresponds to Pe so low that the mixing field is qualitatively different from the other cases. Results for this case are presented only in figure 7 in order to address a specific issue.

Case		Air	Water	Hydrogen, propane
Sc		0.7	600	0.18, 1.2
Re_{jet}	100	10–20 (+)	10–20 (×)	—
	5000	10–30 (□)	10–20 (■)	5–20
	20000	10–20 (○)	10–20 (●)	5–20
	100000	5–10 (△)	—	—

TABLE 1. Cases computed. For each case, the x/D range represented in the figures is shown, with plotting symbols in parentheses where applicable.

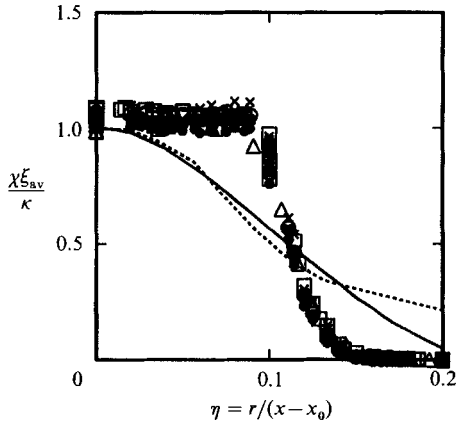

FIGURE 2. Scaled mean mixture fraction $\chi\bar{\xi}(\chi,\eta)/\kappa$, where $\chi = (x-x_0)/D$, versus radial similarity coordinate $\eta = r/(x-x_0)$. Symbols are defined in table 1. Solid curve: measurements by Dowling (1988). Dashed curve: conditioned measurements by Papantoniou (1985).

Figure 2 demonstrates the collapse of the mean-mixture-fraction radial profile to the similarity form $\xi(r,x) = \kappa g(\eta)/\chi$ for the various cases. Here, $\chi = (x-x_0)/D$ is the axial similarity coordinate. Similarity of the computed mean profiles is by no means surprising. It may in fact be regarded as a consistency check on the model because similarity scaling of the stirring field was introduced explicitly.

The constant κ is 3.5 for the computed results. Its experimental value based on an average of Dowling's (1988) measurements (solid curve) in gas at $Re_{jet} = 5000$ and 16000 is 4.9. (The measurements indicate a slight but statistically significant Re-dependence of κ that is as yet unexplained.) Mean profiles have been measured previously by many workers, as cited by Dowling. His measurements are emphasized in the ensuing data comparisons because he has achieved the best spatial resolution to date relative to the scalar fluctuation lengthscale. (Measurements represented by the dashed curve are discussed shortly.)

Unlike Dowling's measured profile, the computed profile exhibits a plateau near the centreline and an abrupt transition to rapid fall-off. To some extent, these features are artifacts of the assumed step-function radial dependence of the inversion-rate parameter λ, which was carried over from the planar-shear-layer formulation (Kerstein 1989). A more gradual radial fall-off of λ, reflecting the radial variation of turbulence intensity in round jets, would have smoothed these features somewhat. Nevertheless, the shape of the computed profile may be qualitatively valid, based on the following considerations.

Despite the contrast between the measured and computed mean profiles,

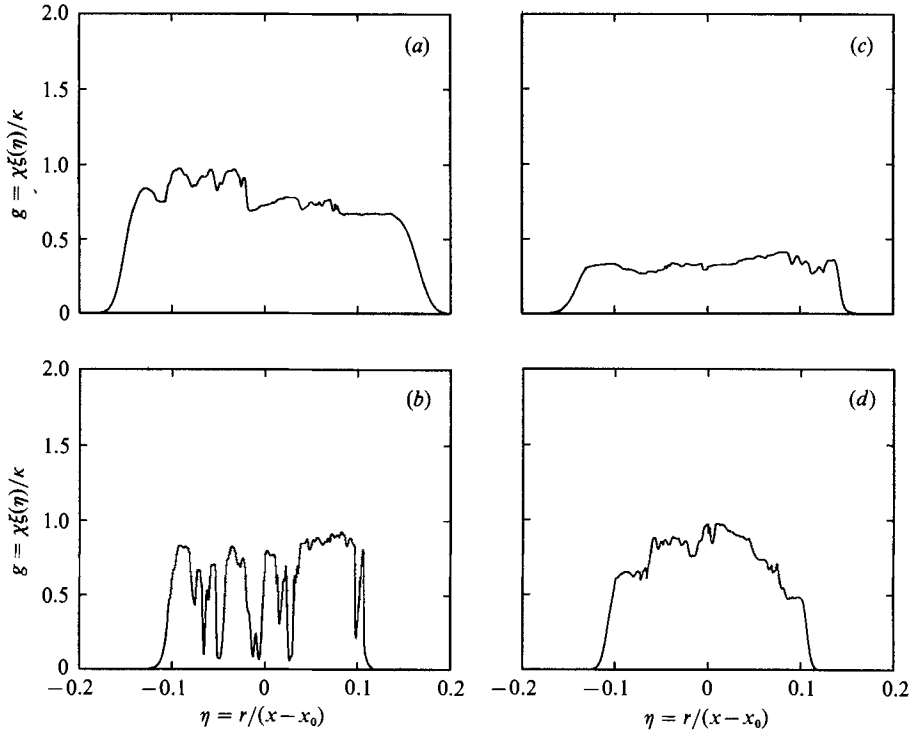

FIGURE 3. Simulated instantaneous radial profiles of scaled mixture fraction $g = \chi\xi(\eta)/\kappa$ at $\chi = 25$ for air ($Sc = 0.7$) at $Re_{\text{jet}} = 5000$.

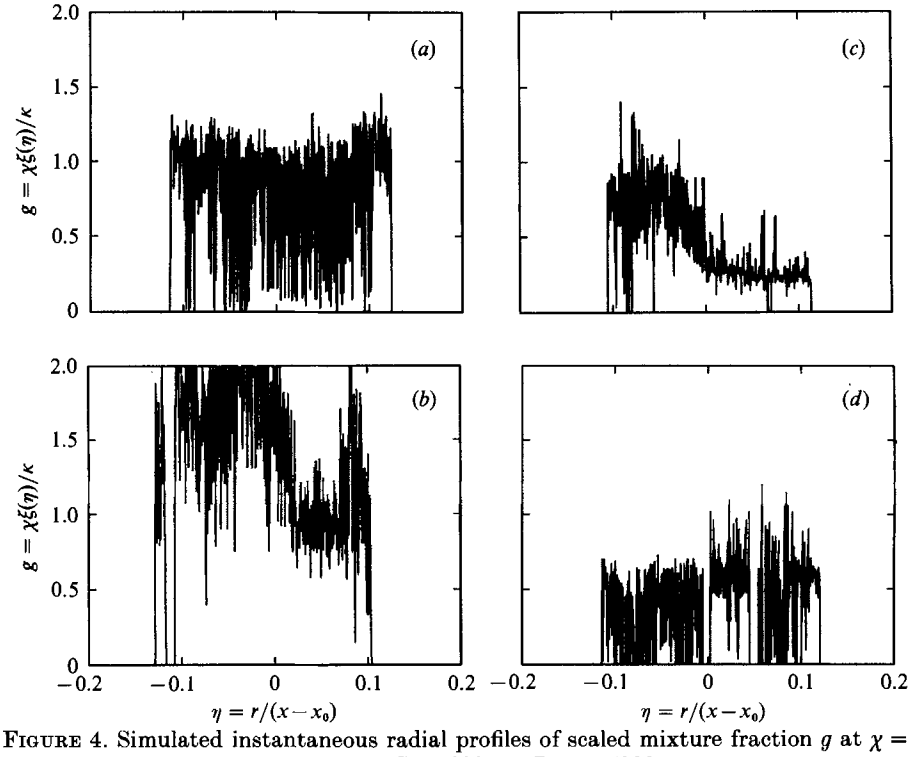

FIGURE 4. Simulated instantaneous radial profiles of scaled mixture fraction g at $\chi = 25$ for water ($Sc = 600$) at $Re_{\text{jet}} = 5000$.

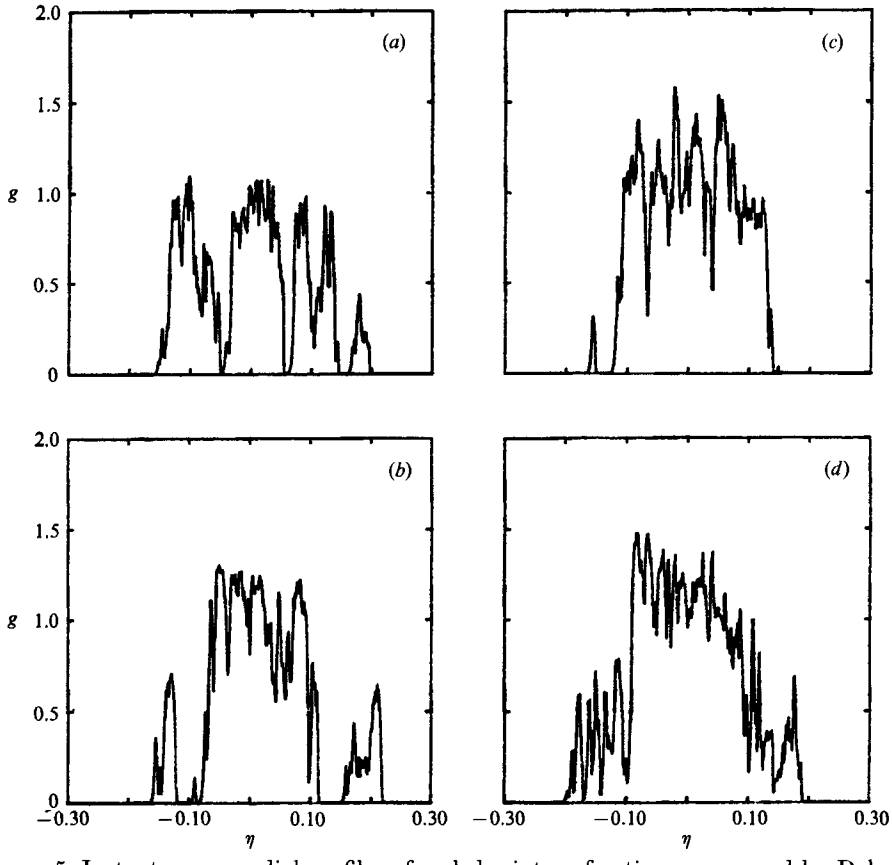

FIGURE 5. Instantaneous radial profiles of scaled mixture fraction g measured by Dahm (1985) at $\chi = 300$ in water ($Sc = 600$) at $Re_{\text{jet}} = 5000$. (Reproduced with permission.)

instantaneous scalar profiles from the simulations exhibit qualitative features consistent with measured instantaneous profiles. Simulated instantaneous profiles are shown in figures 3 and 4 for air and water, respectively. Instantaneous profiles measured in water (Dahm 1985; Dahm & Dimotakis 1987) are shown in figure 5. Computations and measurements both yield instantaneous profiles that exhibit fluctuations about a roughly constant level near the centreline, with relatively sharp drops at the instantaneous boundaries. This 'step-function-plus-noise' picture is confirmed by recent instantaneous-profile measurements by Papantoniou & List (1989) in a liquid jet and by R. W. Dibble (1989, personal communication) and van Cruyningen, Lozano & Hanson (1989) in air jets.

In a study of scalar mixing in planar jets, Uberoi & Singh (1975) obtained instantaneous transverse profiles consistent with this picture. They noted the apparent discrepancy between the trendless noise in the mixed zone and the bell-shaped mean scalar profiles that they obtained, similar in appearance to Dowling's profile in figure 2. Conjecturing that the bell-shaped mean profile reflects transverse displacements of the jet rather than a mixing motion, they formed a conditioned mean profile with the centreline referenced to the instantaneous centre of the mixed zone, thereby correcting for transverse displacements. The conditioned profile they obtained was flat for $|\eta| < 0.1$, breaking sharply to a linear fall-off. (For the planar jet, $\eta = y/(x-x_0)$, where y is the transverse coordinate.)

Imaging studies (Dimotakis, Miake-Lye & Papantoniou 1983) have shown that large-scale motions occur also in round jets at high Re. Therefore Papantoniou (1985) performed the analogous conditioning on instantaneous radial profiles measured in a round jet, obtaining the conditioned mean profile shown in figure 2 (dashed curve). The conditioning flattens the profile only slightly, in contrast to the planar-jet result. Papantoniou conjectured that conditioning based on the instantaneous centres of transverse two-dimensional images of the scalar field would yield a flatter profile. (For the round jet, snapshots along a transverse line cannot be corrected for the component of displacement in the orthogonal transverse direction.)

Transverse displacements of the jet are not included in the linear-eddy model because they do not contribute to mixing. (Mixing is induced by relative motion of fluid elements, but not by overall fluid motion referenced to Euclidean coordinates.) Therefore the computed mean profile ideally should be compared to fully conditioned profiles based on transverse two-dimensional images. Although such measurements have not yet been performed, recent advances in the planar imaging of scalar fields (van Cruyningen *et al.* 1989) should render them feasible in the future.

The key point is that the computed results of figures 2–4 are consistent with the emerging picture of the turbulent jet mixing field. Namely, a spatially uniform, partially mixed state is formed within the interior of the jet, with a fairly abrupt transition to an unmixed state near the edge of the vortical zone.

3.2. *Fluctuation statistics*

Ideally, radial profiles of computed scalar fluctuation statistics should likewise be compared to measured profiles conditioned to correct for transverse displacements. Bearing this caveat in mind, the computed results are compared here to the available, unconditioned fluctuation statistics that have been measured. As noted earlier, the comparisons serve to interpret overall trends, especially Sc effects, rather than detailed features.

The radial profile of the r.m.s. fluctuation of mixture fraction, figure 6, exhibits similarity analogous to figure 2. The occurrence of the peak r.m.s. fluctuation where the slope of the mean profile is greatest is a familiar feature, reproduced by many modelling approaches (Kerstein 1988).

The computed streamwise dependence of the centreline fluctuation intensity $\xi'/\bar{\xi}$ is shown in figure 7. It is apparent that the fluctuation intensity exhibits a χ-dependence whose convergence to a far-field asymptote is slow. Although this extended transient has been observed in many experiments, the high-resolution measurements of Dowling (1988) indicate that the observed transient may have been an artifact of insufficient near-field spatial resolution. In gas, Dowling obtains a far-field asymptote beyond $\chi = 20$, with measured values of 0.23 and 0.24 for $Re_{\text{jet}} =$ 5000 and 16000, respectively.

In figure 7, distinctive transient behaviour is exhibited for the case of liquid at $Re_{\text{jet}} = 20000$. This is the case with the highest Pe and therefore the slowest onset of molecular-diffusive effects. The consequent slow establishment of a convective-diffusive balance is responsible for the high near-field fluctuation intensity in figure 7, and for imperfect compliance with similarity scaling in several subsequent figures. The degree of non-compliance is different for different fluctuation statistics (e.g. note the good collapse to similarity in figures 2 and 6), consistent with the experimental observation that different statistics relax to similarity at different rates (Wygnanski & Fiedler 1969).

Several features of the parametric variation of the computed fluctuation intensity

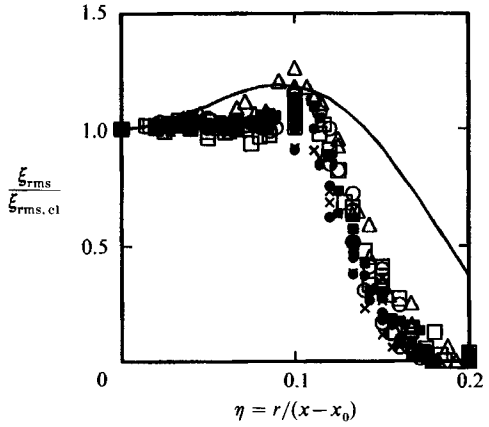

FIGURE 6. Scaled r.m.s. fluctuation of mixture fraction $\xi'(\chi,\eta)/\xi'(\chi,0)$ versus radial similarity coordinate η. Solid curve: measurements by Dowling (1988).

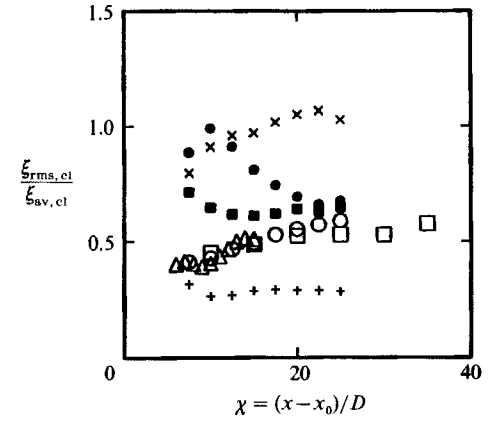

FIGURE 7. Fluctuation intensity of the centreline mixture fraction $\xi'(\chi,0)/\bar{\xi}(\chi,0)$. Symbols are defined in table 1.

are noteworthy. For high Re_{jet}, there is no discernible dependence on Re_{jet} and only a slight dependence on Sc. To further investigate the dependence on Sc, computations were performed for $Re_{jet} = 100$, despite the physical unrealizability of fully developed turbulent flow at this value. Curiously, reduction of Re_{jet} causes a reduction of the fluctuation intensity in air but an increase in water!

The computed behaviour in air can be understood based on an analogy to measured mixing rates in planar shear layers (Broadwell & Dimotakis 1986). A normalized measure of mixing is found in those experiments to decrease with increasing Re in air but remain constant with increasing Re in liquid.

The Re-dependence in air is interpreted as a mixing-rate augmentation whose impact decreases with increasing Re. This augmentation is attributed to molecular-diffusive mixing in the 'internal superlayers' (Effelsberg & Peters 1983) surrounding parcels of free-stream fluid newly entrained into the mixing layer. The narrow regions of large scalar gradient in the lower-left snapshot of figure 3 are realizations of internal superlayers in the simulation. According to the Broadwell–Breidenthal–Mungal (BBM) picture (Broadwell & Breidenthal 1982; Broadwell & Mungal 1988; Broadwell 1988, 1989), the internal-superlayer contribution to the

mixing rate is governed by the large-eddy length- and timescales, and is predicted to vanish as $(ReSc)^{-\frac{1}{2}}$. This contribution augments the mixing based on the classical picture of complete lengthscale breakdown followed by rapid diffusive homogenization. The classical picture yields a Re-independent normalized mixing rate in the similarity regime.

The low-Re effect indicated by the computed results for the gaseous jet may be analogous to the internal-superlayer contribution to gas mixing in shear layers. Namely, mixing enhancement leads to reduction of scalar fluctuations, so the two observations may reflect the same mechanism. In this regard, it is noteworthy that the shear-layer effect was reproduced by the linear-eddy model as applied to that flow (Kerstein 1989).

The computed trend for the jet in water can also be interpreted in the context of the BBM picture. The computed trend may reflect the inability of the low-Re stirring field rapidly to homogenize the entrained fluid upon completion of lengthscale breakdown. The criterion for rapid homogenization (relative to the lengthscale breakdown time) is $Re \gg (\ln Sc)^2$ (Batchelor 1959; Broadwell 1988, 1989). For $Sc = 600$ this requires $Re \gg 40$, which should be compared to the turbulence Reynolds number $Re = 25$ for $Re_{\rm jet} = 100$. Thus, the results for both water and air are consistent with the BBM picture. It should be noted here as previously (Kerstein 1989) that this consistency is an inference based on the computed trends; the assumptions of the BBM picture are not built into the linear-eddy model.

Thus, a large Sc effect is predicted only at $Re_{\rm jet}$ too low to correspond to the fully developed turbulence picture. Based on the results shown in figure 7, there is also the possibility of an observable effect at $Re_{\rm jet}$ of order 10^4. Measurements in water jets (Dahm 1985; Papantoniou 1985) suggest such an effect, but are not definitive. The observation (Drake, Bilger & Stårner 1982) that the fluctuation intensity in a $Re_{\rm jet} = 11\,200$ hydrogen–air jet diffusion flame was larger for seeded-particle ($Sc \gg 1$) than for species-concentration ($Sc < 1$) measurements has been interpreted by Bilger (1989) as a Sc effect in that flow. These experimental results, as well as the computed results of figure 7, indicate that additional high-resolution measurements over a range of Re- and Sc-values are desirable.

A noteworthy feature of the BBM picture is the prediction that dependences of the mixing rate on Re and Sc reduce to a dependence on $Pe = ReSc = D_{\rm T}/D_{\rm M}$, provided that the aforementioned criterion for rapid homogenization is obeyed. It is shown in the ensuing discussion that the present formulation generally exhibits this reduction, with deviations mainly at low Pe.

3.3. *Other scalar properties*

A key property governing the scalar mixing rate is the scalar dissipation $2D_{\rm M}(\nabla\xi)^2$ (Bilger 1976). To estimate the time-average value of this quantity from time records of ξ measured at a fixed location in a gas jet, Dowling (1988) adopts Taylor's frozen-flow hypothesis to obtain $\partial\xi/\partial r$ and assumes isotropy to obtain $\overline{(\nabla\xi)^2} = 3\overline{(\partial\xi/\partial r)^2}$. Adopting the notation $\zeta = (\frac{1}{2}D)^2(\partial\xi/\partial r)^2$, the similarity variable that he uses to plot his measurements can be expressed as $\log_{10}(24\chi^4\bar{\zeta}/Pe_{\rm jet})$, where $Pe_{\rm jet} = ScRe_{\rm jet}$. His measured results for $Re_{\rm jet} = 5000$ and 16000 collapse to a similarity form represented by the solid curve in figure 8, with roughly 20% scatter about this curve based on x/D ranging from 20 to 90.

The computed results for this quantity, also shown in figure 8, exhibit analogous similarity. Although some dependence on Sc and $Re_{\rm jet}$ is apparent, it is a mild dependence in view of the thousandfold variation of each of these parameters among

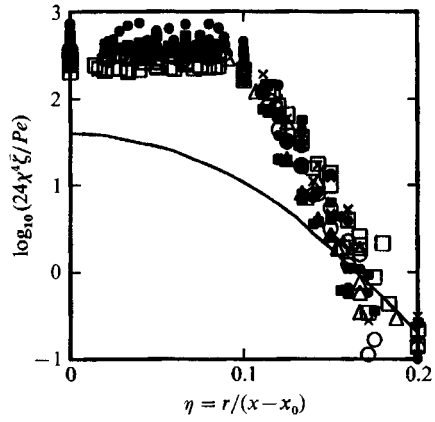

FIGURE 8. $\mathrm{Log}_{10}(24\chi^4\bar{\zeta}/Pe_{\mathrm{jet}})$, where $\zeta = (\frac{1}{2}D)^2(\partial\xi/\partial r)^2$, versus radial similarity coordinate η. Solid curve: measurements by Dowling (1988).

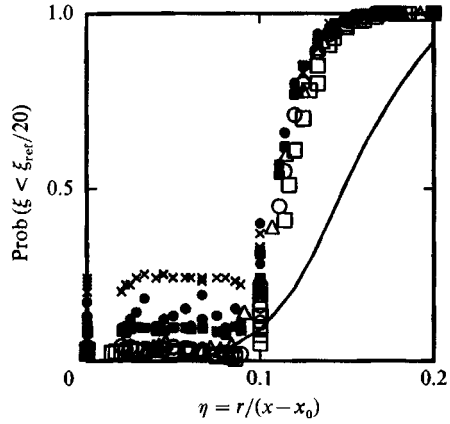

FIGURE 9. Unmixed-fluid probability, $\mathrm{Prob}[\xi < \xi_{\mathrm{ref}}/20]$, where $\xi_{\mathrm{ref}} = \kappa/\chi$, versus radial similarity coordinate η. Symbols are defined in table 1. Solid curve: measurements by Antonia *et al.* (1975).

the various cases, with Pe_{jet} ranging from below 10^4 to above 10^7. The scalar dissipation has not yet been measured in liquid jets, so the similarity with respect to Sc is as yet unverified.

A scalar property that reportedly (Dahm 1985) exhibits significant Sc sensitivity in turbulent jets is the probability of observing pure ambient fluid ($\xi = 0$) at a given location. The solid curve shown in figure 9 represents measurements in air at $Re_{\mathrm{jet}} = 10000$ by Antonia, Prabhu & Stephenson (1975). (That and other studies refer to the probability that $\xi \neq 0$ as the intermittency.) That study as well as Dowling's (1988) measurements in gas indicate negligible penetration of ambient fluid to the centreline. In contrast, Dahm (1985) finds significant (probability 0.13) penetration to the centreline in water at $Re_{\mathrm{jet}} = 5000$.

The operational definition of unmixed fluid suggested by Dahm is adopted here, namely fluid for which ξ is less than 5% of a reference value. The reference value is chosen to be the centreline similarity value κ/χ, where $\kappa = 3.5$ as noted in §3.1. The computed results, shown in figure 9, exhibit a significant Sc-dependence for Re_{jet} of order 10^4. For the case of water at $Re_{\mathrm{jet}} = 20000$, the sequences of points converging

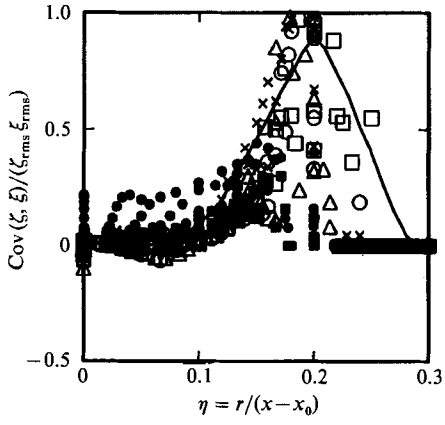

FIGURE 10. Correlation of ξ and ζ, where $\zeta = (\frac{1}{2}D)^2(\partial\xi/\partial r)^2$, versus radial similarity coordinate η. Solid curve: measurements by Namazian *et al.* (1988).

to the better-collapsed results for water at $Re_{\mathrm{jet}} = 5000$ reflect transient relaxation with increasing χ, as discussed in §3.2.

Comparison of water at $Re_{\mathrm{jet}} = 100$ and air at $Re_{\mathrm{jet}} = 10^5$, cases with almost the same Pe_{jet}, suggests that the Sc-dependence does not reduce to a dependence on Pe_{jet}. A countervailing consideration is that the former case does not satisfy the criterion (§3.2) for rapid homogenization, so this may not be a legitimate comparison. Nevertheless, it can be stated that similarity with respect to the unmixed-fluid probability is predicted to be less robust than with respect to, for example, the computed scalar dissipation (figure 8).

A scalar property whose computed Sc-dependence does appear to reduce to a dependence on Pe_{jet} is the correlation coefficient (i.e. the normalized covariance) of ξ and its squared radial derivative ζ. The computed results, shown in figure 10, indicate close correspondence of the correlation profiles for water at $Re_{\mathrm{jet}} = 100$ and air at $Re_{\mathrm{jet}} = 10^5$. The transient relaxation for the case of water at $Re_{\mathrm{jet}} = 20000$ is again evident.

The solid curve is a correlation profile measured by Namazian, Schefer & Kelly (1988) in air for $Re_{\mathrm{jet}} = 7000$. Several caveats should be noted regarding comparison to the measurements. First, the measured correlation involves not ζ but the scalar dissipation, computed from planar scalar maps using an approximate model. Second, all relevant lengthscales may not have been resolved. Third, the correlation profiles, measured at x/D ranging from 5 to 17, exhibited significant departures from similarity, indicating near-field influences and possible effects of marginally adequate spatial resolution. The profile measured at $x/D = 5$ is plotted in figure 10 because it is in best agreement with the computations. For these reasons, the data comparison should be regarded as a demonstration of the physical plausibility of the computed results rather than a validation.

The shape of the correlation profile largely reflects the radial variation of the unmixed-fluid probability. Unmixed fluid tends to introduce positive correlation because both the mixture fraction and its derivative are small in regions with low concentrations of nozzle fluid, reflecting the incomplete lengthscale breakdown of newly entrained fluid parcels.

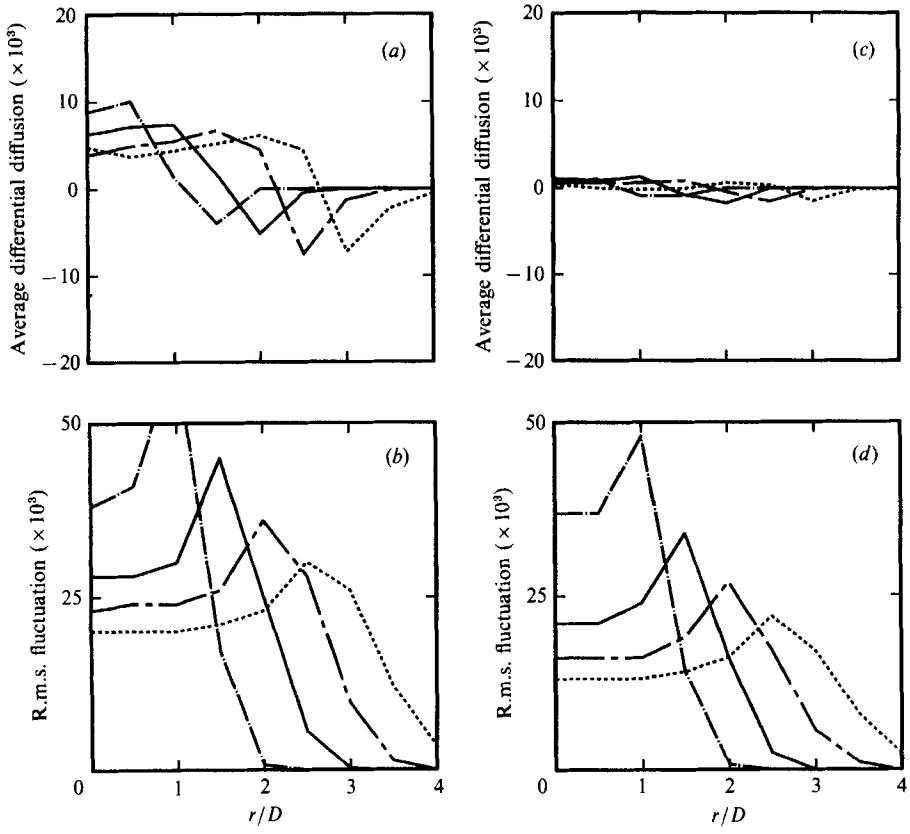

FIGURE 11. Computed radial profiles of mean and r.m.s. differential diffusion for a jet of H_2 and propane into air at (*a*, *b*) $Re_{jet} = 5000$ and (*c*, *d*) $Re_{jet} = 20000$. —·—·—, $x/D = 5$; ——, 10; — — — —, 15; ·····, 20.

4. Differential diffusion

The foregoing comparisons of measured and simulated features of scalar mixing have motivated some physical hypotheses concerning the mixing process. Although the computed results are intuitively reasonable and consistent with measurements, the available scalar mixing measurements are not sufficiently comprehensive or reliable to provide a stringent test of predicted *Sc* effects. Recently reported (Kerstein *et al.* 1989) differential molecular diffusion measurements in a turbulent jet provide such a test. Differential diffusion is an effect whose occurrence at high *Re* is an unambiguous, quantitative indicator of *Sc* sensitivity.

The measurements were performed in a jet of 90% H_2 and 10% Freon-22 (on a molar basis) issuing into air with $Re_{jet} = 20000$. (Freon-22 is $CHClF_2$.) The Rayleigh scattering properties of this gas mixture permitted a direct measurement of the quantity $z = \xi_F - \xi_H$, where ξ_F and ξ_H are the mixture fractions of Freon and H_2, respectively. Here, mixture fraction is defined as species mole fraction normalized by the species mole fraction in the nozzle fluid. (Bilger & Dibble (1982) and others define mixture fraction in terms of mass fractions rather than mole fractions, an approach that is advantageous for modelling but does not yield a unique relationship between differential diffusion and the Rayleigh signal.)

In the computations, these species are treated as passive scalar contaminants,

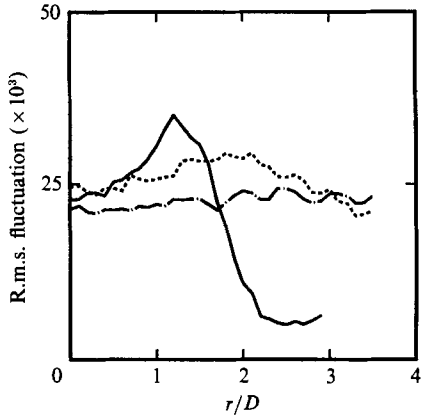

FIGURE 12. Measured radial profiles of r.m.s. differential diffusion for a jet of H_2 and Freon into air at $Re_{jet} = 20000$ (Kerstein *et al.* 1989). ——, $x/D = 10$; ·····, 20; —·—·—, 30.

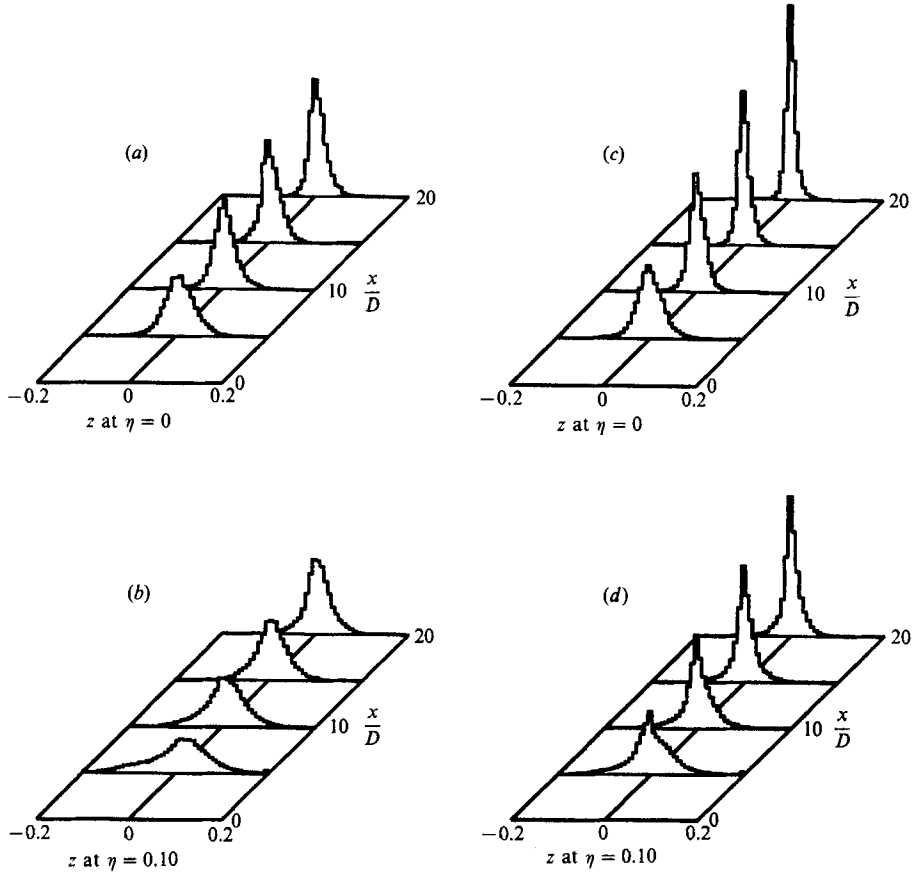

FIGURE 13. Computed centreline ($\eta = 0$) and off-axis ($\eta = 0.1$) probability density functions of differential diffusion z for a jet of H_2 and propane into air at (*a*, *b*) $Re_{jet} = 5000$ and (*c*, *d*) $Re_{jet} = 20000$.

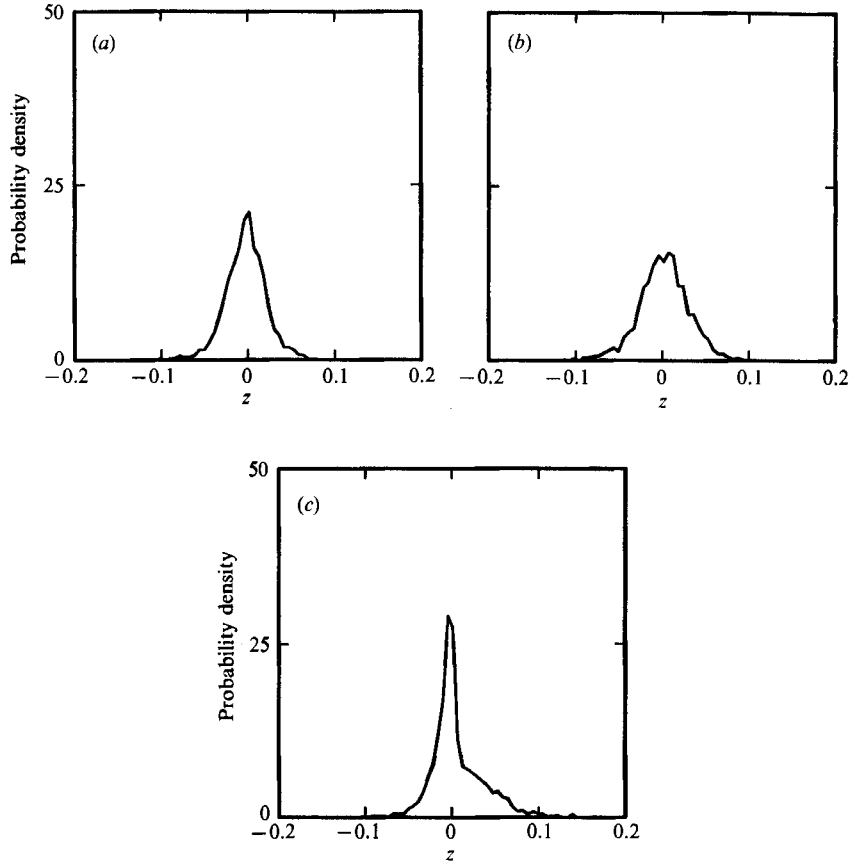

FIGURE 14. Measured probability density functions of differential diffusion z at $x/D = 10$ for a jet of H_2 and Freon into air at $Re_{jet} = 20000$, for r/D values (*a*) 0, (*b*) 0.9, and (*c*) 1.6 (Kerstein *et al.* 1989).

neglecting the possible dynamical consequences of density fluctuations and non-Fickian molecular transport. Therefore the model is most directly applicable to an air jet with trace concentrations of H_2 and Freon, although it is applied here to measurements involving high concentrations, especially of the latter.

As indicated in table 1, computations were performed based on the respective *Sc* values for H_2 and propane (rather than Freon). This choice facilitates comparison to a previous (Bilger & Dibble 1982) differential-diffusion analysis that adopted H_2–propane as a test case.

Profiles of $\tilde{z}$ and z'' computed for $Re_{jet} = 5000$ and 20000, respectively, are shown in figure 11. Comparison of these two cases indicates that the mean profiles scale inversely with Re_{jet}, while the r.m.s. profiles are much less sensitive to Re_{jet}. These features are also obtained by Bilger & Dibble (1982), based on estimates of the leading terms in their gradient-transport model. (Namely, generation of mean z scales as the higher of the two molecular diffusivities. Mean z is dissipated by turbulent mixing, so z-dissipation scales as the turbulent diffusivity, yielding a balance level $z \sim Re_{jet}^{-1}$. Fluctuations of z are generated and dissipated by turbulent mixing and hence the r.m.s. profiles remain finite at high Re_{jet}.) The profile shapes that they obtain are likewise comparable, except that their mean profiles peak at the

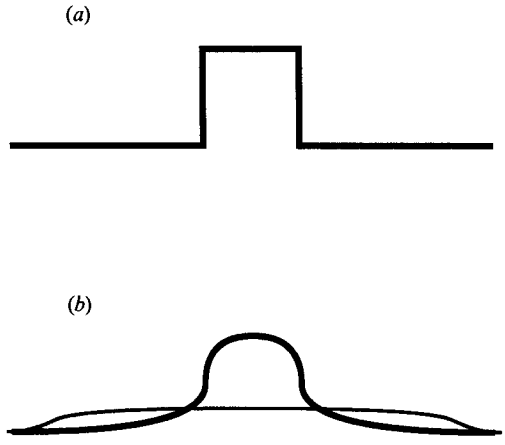

FIGURE 15. Schematic interpretation of the asymmetry of the probability density function of differential diffusion. (*a*) Initial radial profile of mixture fraction for both species, resulting from the transport of a packet of nozzle fluid into the outer fluid. (*b*) Subsequent profiles of mixture fraction for the slow-diffusing species (heavy curve) and the fast-diffusing species (light curve).

centreline. The key difference between the predictions is that Bilger & Dibble (1982) obtain mean values that typically exceed the r.m.s. fluctuations by a factor of 2 or more for Re_{jet} of order 10^4, while the present computations yield mean values much smaller than the r.m.s. fluctuations.

The present computations are in good agreement with the measurements by Kerstein *et al.* (1989). Agreement with measured fluctuation profiles is indicated by comparison of figure 11 to measured profiles shown in figure 12. Measured profiles of the mean differential diffusion never exceeded the measurement noise threshold of 0.007. Consistent with this observation, the computed mean profiles for $Re_{\text{jet}} = 20000$ fall well below this threshold.

Insight into the mechanism of differential diffusion is gained by examination of spatially resolved p.d.f.'s of z. An interesting feature not revealed by examination of the mean and r.m.s.-fluctuation profiles is the asymmetry of both computed (figure 13) and measured (figure 14) p.d.f.'s, especially noticeable at large radial offsets.

A mechanistic interpretation of this observation is schematically illustrated in figure 15. The initial scalar profile in that figure represents a parcel of fluid that has been transported by a large eddy from the vicinity of the centreline to its present location near the edge of the jet. The parcel contains high concentrations of both the fast- and the slow-diffusing species, while the surrounding fluid has neither. After a time interval short compared to convective times, molecular diffusion has spread the fast-diffusing species over a broader range than the slow-diffusing species. If the original parcel is smaller than the zone now containing the fast-diffusing species, then the scalar profiles develop as in figure 15. Namely, a small zone has a large excess of the slow-diffusing species, corresponding to large, positive z, while a large zone has a small excess of the fast-diffusing species, corresponding to small, negative z. This implies a p.d.f. that is long-tailed with respect to positive z.

This interpretation implies a subtle relationship between flow-field properties (sizes of convected parcels, convection times, etc.) and statistical properties of the quantity z. The possibility that measured properties of z provide useful information about the flow field, beyond the specific issue of scalar mixing addressed here, merits further investigation.

5. Two-source correlation

Many of issues addressed thus far with regard to jet mixing are likewise pertinent to other turbulent flows. In a previous application of the linear-eddy approach (Kerstein 1988), some of these issues were considered with reference to scalar mixing in grid turbulence. The next issue that is considered concerns an interesting observation in grid turbulence by Warhaft (1984) that may be pertinent to jets and other free-shear flows.

Warhaft measured the fluctuation statistics of the thermal field downstream of one or more parallel heated wires behind a grid in a wind tunnel. The wires were fixed in a plane transverse to the mean flow. By analysing measurements involving one and two wires, respectively, Warhaft achieved the thermal analogue of the following measurement. In the two-wire configuration, suppose that the wires are sources of distinct, equal-diffusivity species A and B, respectively. Downstream of the wires, Warhaft obtained, in effect, the spatially resolved correlation coefficient $\rho = \mathrm{cov}\,(c_A c_B)/[\mathrm{var}\,(c_A)\,\mathrm{var}\,(c_B)]^{\frac{1}{2}}$ in the plane equidistant from the wires. As a function of streamwise distance x from the wires, Warhaft observed that ρ exhibited complicated behaviour in the near field, followed by relaxation to an apparent asymptote less than unity. (The observed asymptote was not definitive due to the limited streamwise range of the measurements.) Sawford (1985) showed that Durbin's (1980) particle-dispersion model reproduces the qualitative effect, including the dependence of the asymptote on the ratio of the wire separation to the turbulence integral scale.

A non-unity asymptote would imply incomplete mixing of A and B in the far field. This effect, if observed likewise in jets, would have the following implication. The fluctuation intensity (figure 7) is presumably maintained at a constant level by the continual entrainment of unmixed fluid into the vortical zone. Warhaft's effect would imply that two entrained fluid parcels would not fully mix with each other, let alone with fresh fluid, indefinitely far downstream. Incomplete mixing is possible owing to the continual transverse spreading of the vortical zone, causing some separation between convected elements of the respective parcels to be maintained despite the stirring-induced lengthscale reduction.

To test this possibility computationally, simulations were run with two distinct equal-diffusivity scalars A and B with respective initial conditions $\xi_A = 1$ for $0.99(\frac{1}{2}D) < |r| < \frac{1}{2}D$, otherwise zero, and $\xi_B = 1$ for $|r| < (0.02)^{\frac{1}{2}}(\frac{1}{2}D)$, otherwise zero. This initial condition represents a nozzle consisting of three concentric rings, with pure ambient fluid (containing neither A nor B) issuing from the intermediate ring, as illustrated in figure 16. The stated initial conditions correspond to inner and outer ring cross-sections each equal to 2% of the total nozzle cross-section. Other configurations would also be suitable, and could readily be simulated for comparison to measurements.

Two cases were computed, air ($Sc = 0.7$) and water ($Sc = 600$), both at $Re_{\mathrm{jet}} = 5000$. Computed radial profiles of ρ are shown in figure 17. It is apparent that the results for gas are not yet converged to similarity form at small η. Transient relaxation at the centreline is shown in figure 18. For liquid, ρ is converging to a value greater than zero, but much less than unity. (Note the expanded vertical scale.) The asymptote for gas is not evident. Nevertheless, the liquid results demonstrate that the asymptote can be less than unity, and the comparison of cases indicates a significant Sc effect.

Consideration of limiting cases provides a frame of reference for interpreting the results. In the absence of molecular diffusion, the correlation must always be

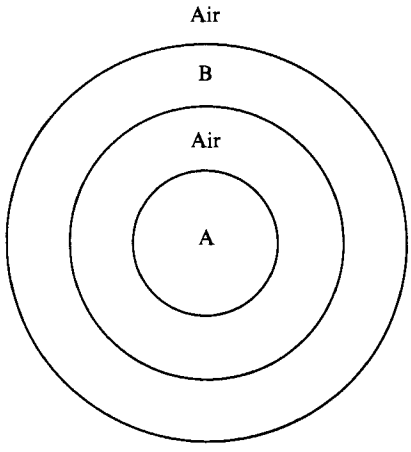

FIGURE 16. Nozzle cross-section for the proposed two-source experiment (not to scale). Tracer species are A and B, respectively.

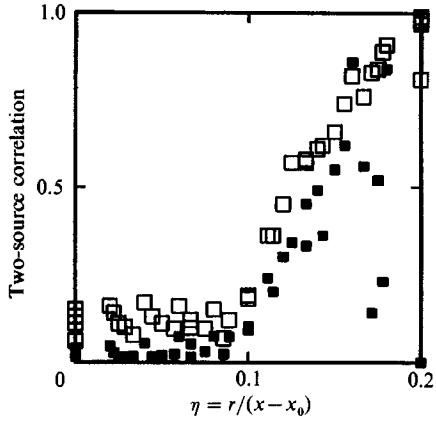

FIGURE 17. Radial profile of the correlation of species A and B, computed for the nozzle configuration of figure 16. Symbols are defined in table 1 (but the x/D range is 10–20 for gas as well as liquid).

negative because A and B never comingle at a point. Positive values for liquid as well as for gas thus indicate a significant influence of molecular diffusion in both cases. In the strongly diffusive limit, i.e. small Pe, the correlation tends to unity. Figure 17 indicates values near unity at the edge of the jet. This may be interpreted as the effect of local Pe. Relatively few block-inversion events subsume the region near the edge so Pe is effectively smaller there.

Except near the edge, the far-field correlation predicted for the jet is lower than that measured by Warhaft. This is to be expected, both because Pe is larger in the present case, and because dilution by fluid entrainment is more effective in the axisymmetric configuration than in Warhaft's line-source configuration.

Near-field behaviour depends on the source configuration. Figure 18 indicates that the asymptote is approached from below, consistent with Warhaft's measurements and his inference that molecular diffusion does not affect ρ in the near field owing to the physical separation of the sources, so the near-field correlation is negative. The relative insensitivity of ρ to Sc in the near field, indicated in figure 18, is also consistent with this inference.

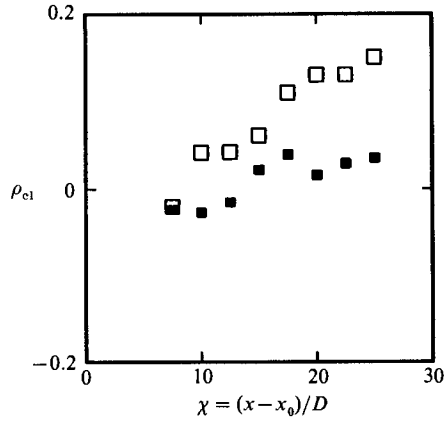

FIGURE 18. Axial profile of the centreline correlation of species A and B, computed for the nozzle configuration of figure 16. (Note the expanded vertical scale.)

The approach to the asymptote from below is also predicted by Durbin's (1980) model (Sawford 1985). A difficulty with that analysis is its prediction of positive values of ρ in the absence of molecular diffusion, reflecting the absence of a mechanistic distinction between molecular diffusion and fine-scale stirring. A discussion of this and subsequent particle-dispersion formulations in this regard is provided elsewhere (Kerstein 1988).

Returning to the computed far-field behaviour, the key inference is that mixing of fluid elements in the jet interior may be incomplete, irrespective of the time available for mixing. For given Re, the ultimate extent of mixing is predicted to depend on Sc.

6. Discussion

It has been demonstrated that a formulation of the linear-eddy model incorporating the geometry and similarity scalings of the self-preserving round jet reproduces many aspects of the scalar fluctuation statistics measured in turbulent jets. The present approach may be viewed as complementary to approaches, surveyed by Pope (1985) and Bilger (1989), that undertake the more ambitious task of simultaneously predicting the turbulent flow field and the scalar field. Those approaches lead to models that are more complicated overall than the present formulation, but embody a less detailed representation of small-scale mixing. Consequently, no one model has previously addressed the wide range of Sc as well as Re and the wide variety of mixing properties considered here.

A general feature of the results and data comparisons presented here is the collapse of the Sc- and Re-dependences to a dependence on $Pe = ScRe$ in most cases. With regard to this and other features, it has been noted that the linear-eddy model is generally consistent with the Broadwell–Breidenthal–Mungal (BBM) picture of scalar mixing in turbulent free shear flows (Broadwell & Breidenthal 1982; Broadwell & Mungal 1988; Broadwell 1988, 1989), although the assumptions of that picture are not built into the linear-eddy model.

Consistency with the BBM picture is a consequence of the development of internal superlayers in the simulated mixing field through the combined influence of large eddies transporting fresh fluid parcels inward and small eddies breaking up the parcels. The Sc-dependence of the mixing rate within these superlayers is captured

by the model because molecular diffusion is incorporated as a distinct mechanism, implemented in a physically sound manner.

Limitations of the available experimental data have been noted with regard to several issues that have been addressed. It is hoped that the capability demonstrated here to model the dependence of jet mixing on *Sc* as well as on *Re* will motivate further high-resolution measurements of the scalar fluctuation intensity, unmixed-fluid probability, and scalar dissipation for diverse conditions. The desirability of measured radial profiles of mean and fluctuating scalar quantities conditioned to remove transverse displacements has been noted. A jet analogue of Warhaft's (1984) two-source correlation experiment in grid turbulence has been proposed and simulated, again in the hope of motivating further measurements. The latter computation suggests a novel mechanistic basis for *Sc*-dependence of the mixing rate.

A feature common to the two-source computation, the differential-diffusion computation, and finite-rate chemistry problems considered previously (Kerstein 1989) is that two or more independent scalars are needed for a complete characterization of the process. It is evident that such multivariate scalar fields arise in a variety of problems, with molecular diffusion serving as a source of scalar fluctuations in the case of differential diffusion. For all the aforementioned problems, linear-eddy computations reveal distinctive features. The asymmetric p.d.f.'s of differential diffusion, the incomplete mixing of distinct components of the nozzle fluid, and the factorization (Kerstein 1989) of chemical product dependences on *Pe* and *Da* are predicted features of fundamental interest that merit additional experimental study.

The issues addressed here are of practical as well as fundamental interest. For example, concentration-field statistics are most conveniently measured in many flows using seeded particles or other tracers with *Sc* far different from the species of interest for predicting chemical reactions (Bilger 1989). Therefore a model with the capabilities demonstrated here may be needed in order to extrapolate from measured concentration statistics to those governing the chemical reaction rate.

Finally, implications of the present and previous applications of the linear-eddy approach are considered with regard to invariant modelling concepts for turbulent mixing. In these applications, an effort has been made to keep configuration-specific modelling inputs to a minimum. It is encouraging that this approach has succeeded in reproducing key trends and features of scalar mixing measured in grid turbulence, planar shear layers, and round jets, despite the well-known idiosyncracies of these flows, such as the coherent structures observed in mixing layers (Brown & Roshko 1974). This suggests that the principal influence of flow geometry on scalar mixing properties at high *Re* is embodied in the similarity laws (or an equivalent description of large-scale evolution) which determine the length- and timescales for convective stirring in accordance with the Kolmogorov inertial-range cascade.

The author would like to thank R. W. Bilger, J. E. Broadwell, W. J. A. Dahm, P. E. Dimotakis and M. G. Mungal for stimulating and helpful discussions, and R. W. Dibble and I. van Cruyningen for sharing results prior to publication. This research was supported by the Division of Chemical Sciences and the Division of Engineering and Geosciences, Office of Basic Energy Sciences, US Department of Energy.

REFERENCES

ANTONIA, R. A., PRABHU, A. & STEPHENSON, S. E. 1975 Conditionally sampled measurements in a heated turbulent jet. *J. Fluid Mech.* **72**, 455–480.

BATCHELOR, G. K. 1959 Small-scale variation of convected quantities like temperature in turbulent fluid. Part 1. General discussion and the case of small conductivity. *J. Fluid Mech.* **5**, 113–133.

BILGER, R. W. 1976 The structure of diffusion flames. *Combust. Sci. Technol.* **13**, 155–170.

BILGER, R. W. 1989 Turbulent diffusion flames. *Ann. Rev. Fluid Mech.* **21**, 101–135.

BILGER, R. W. & DIBBLE, R. W. 1982 Differential molecular diffusion effects in turbulent mixing. *Combust. Sci. Technol.* **28**, 161–172.

BROADWELL, J. E. 1988 Molecular mixing and chemical reactions in turbulent shear flows. In *Disorder and Mixing: Diffusion, Convection, and Reaction* (ed. E. Guyon, Y. Pomeau, E. Charlaix & J.-P. Nadal), Part 5. Martinus Nijhoff.

BROADWELL, J. E. 1989 A model for reactions in turbulent jets: Effects of Reynolds, Schmidt, and Damköhler numbers. In *Turbulent Reactive Flows* (ed. R. Borghi & S. N. B. Murthy), p. 257. Springer.

BROADWELL, J. E. & BREIDENTHAL, R. E. 1982 A simple model of mixing and chemical reaction in a turbulent shear layer. *J. Fluid Mech.* **125**, 397–410.

BROADWELL, J. E. & DIMOTAKIS, P. E. 1986 Implications of recent experimental results for modeling reactions in turbulent flows. *AIAA J.* **24**, 885–889.

BROADWELL, J. E. & MUNGAL, M. G. 1988 Molecular mixing and chemical reactions in turbulent shear layers. In *22nd Symp. (Intl) on Combustion*, pp. 579–587. The Combustion Institute.

BROWN, G. L. & ROSHKO, A. 1974 On density effects and large structures in turbulent mixing layers. *J. Fluid Mech.* **64**, 775–816.

CRUYNINGEN, I. VAN, LOZANO, A. & HANSON, R. K. 1989 Interpretation of planar laser-induced fluorescence flowfield images. *Proc. ASME Winter Conf.* (in press).

CURL, R. L. 1963 Dispersed phase mixing: I. Theory and effects in simple reactors. *AIChE J.* **9**, 175–181.

DAHM, W. J. A. 1985 Experiments on entrainment, mixing and chemical reactions in turbulent jets at large Schmidt numbers. Ph.D. thesis, Caltech.

DAHM, W. J. A. & DIMOTAKIS, P. E. 1987 Measurements of entrainment and mixing in turbulent jets. *AIAA J.* **25**, 1216–1223.

DIMOTAKIS, P. E., MIAKE-LYE, R. C. & PAPANTONIOU, D. A. 1983 Structure and dynamics of round turbulent jets. *Phys. Fluids* **26**, 3185–3192.

DOWLING, D. R. 1988 Mixing in gas phase turbulent jets. Ph.D. thesis, Caltech.

DOWLING, D. R. & DIMOTAKIS, P. E. 1990 Similarity of the concentration field of gas-phase turbulent jets. *J. Fluid Mech.* (in press).

DRAKE, M. C., BILGER, R. W. & STÅRNER, S. H. 1982 Raman measurements and conserved scalar modeling in turbulent diffusion flames. In *19th Symp. (Intl) on Combustion*, pp. 459–467. The Combustion Institute.

DURBIN, P. A. 1980 A stochastic model of two-particle dispersion and concentration fluctuations in homogeneous turbulence. *J. Fluid Mech.* **100**, 279–302.

EFFELSBERG, E. & PETERS, N. 1983 A composite model for the conserved scalar pdf. *Combust. Flame* **50**, 351–360.

GIVI, P., RAMOS, J. I. & SIRIGNANO, W. A. 1985 Probability density function calculations in turbulent chemically reacting round jets, mixing layers and one-dimensional reactors. *J. Non-Equilib. Thermodyn.* **10**, 75–104.

GOULDIN, F. C., SCHEFER, R. W., JOHNSTON, S. C. & KOLLMANN, W. 1986 Nonreacting turbulent mixing flows. *Prog. Energy Combust. Sci.* **12**, 257–303.

KERSTEIN, A. R. 1986 Computational study of propagating fronts in a lattice-gas model. *J. Statist. Phys.* **45**, 921–931.

KERSTEIN, A. R. 1988 A linear-eddy model of turbulent scalar transport and mixing. *Combust. Sci. Technol.* **60**, 391–421.

KERSTEIN, A. R. 1989 Linear-eddy modeling of turbulent transport. II: Application to shear layer mixing. *Combust. Flame* **75**, 397–413.

KERSTEIN, A. R., DIBBLE, R. W., LONG, M. B., YIP, B. & LYONS, K. 1989 Measurement and computation of differential molecular diffusion in a turbulent jet. In *Proc. 7th Symp. on Turb. Shear Flows*, paper 14-2.

LANDAU, L. D. & LIFSHITZ, E. M. 1959 *Fluid Mechanics*, pp. 130–134. Pergamon.

NAMAZIAN, M., SCHEFER, R. W. & KELLY, J. 1988 Scalar dissipation measurements in the developing region of a jet. *Combust. Flame* **74**, 161–170.

PAPANTONIOU, D. A. 1985 Observations in turbulent buoyant jets by use of laser-induced fluorescence. Ph.D. thesis, Caltech.

PAPANTONIOU, D. A. & LIST, E. J. 1989 Large-scale structure in the far field of buoyant jets. *J. Fluid Mech.* **209**, 151–190.

POPE, S. B. 1985 Pdf methods for turbulent reactive flows. *Prog. Energy Combust. Sci.* **11**, 119–192.

SAWFORD, B. L. 1985 Lagrangian statistical simulation of concentration mean and fluctuation fields. *J. Clim. Appl. Met.* **24**, 1152–1166.

UBEROI, M. S. & SINGH, P. I. 1975 Turbulent mixing in a two-dimensional jet. *Phys. Fluids* **18**, 764–769.

WARHAFT, Z. 1984 The interference of thermal fields from line sources in grid turbulence. *J. Fluid Mech.* **144**, 363–387.

WYGNANSKI, I. & FIEDLER, H. 1969 Some measurements in the self-preserving jet. *J. Fluid Mech.* **38**, 577–612.